

Article

Modified Zeolite Catalyst for a NO_x Selective Catalytic Reduction Process in Nitric Acid Plants

Magdalena Saramok ^{1,*}, Agnieszka Szymaszek ², Marek Inger ^{1,*}, Katarzyna Antoniak-Jurak ¹,
Bogdan Samojeden ² and Monika Motak ²

¹ Łukasiewicz Research Network—New Chemical Syntheses Institute, Al. Tysiąclecia Państwa Polskiego 13a, 24-110 Puławy, Poland; katarzyna.antoniak@ins.lukasiewicz.gov.pl

² Faculty of Energy and Fuels, AGH University of Science and Technology, Al. Mickiewicza 30, 30-059 Kraków, Poland; agnszym@agh.edu.pl (A.S.); bsamo1@agh.edu.pl (B.S.); motakm@agh.edu.pl (M.M.)

* Correspondence: magdalena.saramok@ins.lukasiewicz.gov.pl (M.S.); marek.inger@ins.lukasiewicz.gov.pl (M.I.); Tel.: +48-8147-31715 (M.S.); +48-8147-31415 (M.I.)

Abstract: Natural zeolite of the heulandite-type framework was modified with iron and tested as a catalyst for the selective catalytic reduction of nitrogen oxides with ammonia (NH₃-SCR) in the temperature range of 150–450 °C. The catalyst was prepared at a laboratory scale in a powder form and then the series of experiments of its shaping into tablets was conducted. Physicochemical studies of the catalyst (N₂ sorption at –196 °C, FT-IR, XRD, UV-vis) were performed to determine the textural and structural properties and identify the surface functional groups, the crystalline structure of the catalysts and the form and aggregation of the active phase. The activity tests over the shaped catalyst were performed under industry-reflecting conditions, using tail gases from the pilot nitric acid plant. The influence of a temperature, catalyst load, and the amount of reducing agent (ammonia) on the NO_x reduction process were investigated. The results of catalytic tests that were performed on model gas mixture showed that non-modified clinoptilolite exhibited around 58% conversion of NO at 450 °C. The temperature window of the shaped catalyst shifted to a higher temperature range in comparison to the powder sample. The catalytic performance of the shaped Fe-clinoptilolite in the industry-reflecting conditions was satisfactory, especially at 450 °C. Additionally, it was observed that the ratio of N₂O concentration downstream and upstream of the catalytic bed was below 1, which indicated that the catalyst exhibited activity in both DeNO_x and DeN₂O process.

Keywords: nitric acid plant; selective catalytic reduction; zeolite catalyst; iron modified clinoptilolite



Citation: Saramok, M.; Szymaszek, A.; Inger, M.; Antoniak-Jurak, K.; Samojeden, B.; Motak, M. Modified Zeolite Catalyst for a NO_x Selective Catalytic Reduction Process in Nitric Acid Plants. *Catalysts* **2021**, *11*, 450. <https://doi.org/10.3390/catal11040450>

Academic Editor: Feng Gao

Received: 8 March 2021

Accepted: 27 March 2021

Published: 31 March 2021

Publisher's Note: MDPI stays neutral with regard to jurisdictional claims in published maps and institutional affiliations.

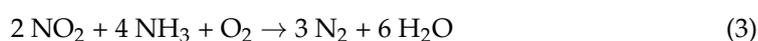
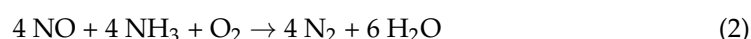
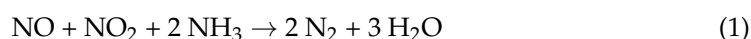


Copyright: © 2021 by the authors. Licensee MDPI, Basel, Switzerland. This article is an open access article distributed under the terms and conditions of the Creative Commons Attribution (CC BY) license (<https://creativecommons.org/licenses/by/4.0/>).

1. Introduction

The worldwide production of nitric acid (HNO₃) reaches around 55 million tons per year. Approximately 80% of the product is processed into nitrogen fertilizers, mainly ammonium nitrate [1]. The rest of the acid is utilized as an intermediate product for the synthesis of various chemicals, such as caprolactam, adipic acid, or dinitrotoluene. Nitric acid is very important feedstock in many industrial processes, but its production results in the emission of significant amount of harmful gases, mainly nitrogen monoxide (NO) and nitrogen dioxide (NO₂), which are summarily referred to as NO_x and N₂O, being ranked among the greenhouse gases. NO_x can cause serious health damage, including respiratory and cardiovascular diseases. Additionally, NO_x contributes to the formation of acid rain and ground-level ozone, which can damage ecosystems, acting harmfully to animal health and affecting the vegetative processes of plants. Moreover, they are also responsible for the photochemical smog formation, poor air quality in larger metropolitan areas, and acceleration of metal corrosion. Therefore, there is a need for a further-tightening-up of the nitrogen oxides emission limits, defined under the Directive of the European Parliament. Currently, NO_x emission standards for the new and existing nitric acid plants are set at the level of 75 and 90 ppm, respectively. Nevertheless, the maximum permitted emission level

is up to 150 ppm if there is a risk of ammonium nitrates deposition in the selective catalytic reduction (SCR) unit, which limits the efficiency of SCR process [2,3]. Several methods of NO_x emission abatement from nitric acid plants are known, such as highly efficient absorption, non-selective catalytic reduction (NSCR), selective catalytic reduction (SCR), and absorption in sodium hydroxide solution [3]. The most efficient technology is selective catalytic reduction, which involves the reaction between nitrogen oxides and ammonia that, in most cases, acts as the reducing agent (NH₃-SCR). “Selectivity” of ammonia means that it reacts with NO and NO₂ first, and then with O₂. The mechanism of NH₃-SCR depends on the operating window of the catalyst, O₂ content, and NO₂/NO_x ratio in the tail gas stream. Because of that, different reactions may take place during the process Equations (1)–(3) [4,5]:



The reaction that is described by Equation (1) proceeds mainly in the presence of equimolar amount of NO and NO₂ in the tail gas stream, while the reaction that is represented by Equation (2) demands the excess of oxygen [6]. The reactor for the SCR process can be installed upstream or downstream of the tail gas expansion turbine. In mono-pressure nitric acid plants, where the temperature of the tail gas is lower, many types of catalysts that exhibit satisfactory activity in the temperature range of 200–300 °C can be used (for example, noble or transition metals supported on the ceramic support) [7]. Below this temperature range, the undesirable process of the formation of ammonium salts can occur. These compounds accumulate in the cooler zones of the plant and are highly dangerous due to their explosive character [8–10]. In dual-pressure plants, where two different pressures are used in the oxidation and absorption units, the tail gas has a higher temperature that usually exceeds 300 °C. The catalyst that is used in this temperature range should be resistant to thermal deactivation and in this case, good examples are vanadium-based catalyst, for example V₂O₅-WO₃ (MoO₃)-TiO₂ and modified zeolites [11]. However, the problem is a considerable decrease in selectivity of the material above 350 °C caused by side reactions, such as oxidation of ammonia to NO and the formation of N₂O. The interesting solution of that problem is simultaneous removal of NO_x and N₂O from tail gas in one reactor [12–14]. The final effect of NO_x reduction can be used to increase the tail gas temperature upstream of DeN₂O catalyst bed, which is beneficial for DeN₂O catalyst operation.

NC-300 is one of the commercial catalysts dedicated for nitric acid plants. It consists of SiO₂, Al₂O₃, Fe₂O₃, and K₂O. This catalyst reaches NO_x reduction above 90% in the temperature range of 260–370 °C, in the presence of oxygen in the gas stream [15]. Nevertheless, in the modern designed nitric acid plants, the tail gas temperature upstream of the expansion turbine, where the SCR reactor is installed, can reach 430 °C, and not all commercial catalysts are equally effective at this temperature. V₂O₅ deposited on the support consisting of TiO₂, Al₂O₃, or SiO₂ is the most popular commercial catalyst used in nitric acid plants. The catalysts containing WO₃ and/or MoO₃, known from patents [16–18], are very effective in the SCR process. The addition of molybdenum and/or tungsten improves the activity and selectivity of the catalytic system. Moreover, WO₃ works as a structural stabilizer and it increases the thermal stability of the material. The operating temperature window of vanadia catalysts, in which more than a 90% NO_x reduction is reached, is 300–400 °C. The high cost of V₂O₅ and TiO₂ is the disadvantage of such systems.

An alternative idea for the substitutive catalyst for nitric acid plant are precious metals that are deposited on ceramic supports, for example Pt-Rh/γ-Al₂O₃. The system is highly active in the SCR process, but the use of noble metals in nitric acid plants is operationally unfavorable due to the high cost of the catalysts and their low selectivity to N₂ [19–21]. Many innovative supports have been proposed in the scientific literature so far, such as acti-

vated carbon [22,23], carbon nanotubes [24,25], layered double hydroxides [26,27], layered clays [28–31], and zeolites [32–36]. Among them, significant attention was paid to zeolites that are microporous aluminosilicate minerals, either naturally occurring or industrially produced on a large scale. The crystallographic structure of zeolites is formed by a three-dimensional network of alumina [AlO₄] and silica [SiO₄] tetrahedrons, interconnected in various ways and forming channels and cells. The presence of channels and pores (channel entrances) in the zeolites structure is beneficial for the sorption and catalytic properties. The modification of zeolites with various metals is often performed to increase the activity and selectivity of this material [16,37,38]. Many different zeolite-based catalysts for SCR process are reported in the literature. They are mainly based on materials with a high content of Si, such as MFI, BEA, FER, MOR, FAU, MEL, modified with metals, for instance, cobalt (Co-ZSM-5 [16]), copper (Cu-SSZ-13 [38], Cu-CHA [39], Cu-ZSM-34 [40]), or iron (Fe-BEA [37], Fe-ZSM-5 [41]).

Among natural zeolites, clinoptilolite is an interesting candidate for the support of the novel NH₃-SCR catalyst [29,34,42]. Its general chemical formula is (Na,K)₆Al₆Si₃₀O₇₂·20 H₂O [43] and it is the most abundant natural zeolite of the heulandite-type framework (HEU). Deposits of clinoptilolite can be found, for example, in Slovakia, Hungary, China, Iran, New Zealand, Argentina, and Cuba [43–45]. Clinoptilolite possesses the exceptional physical properties, which it owes to its two-dimensional structure [46]. Additionally, exhibits high mechanical crush strength (more than 7 MPa), which is crucial for its stability during the majority of catalytic reactions [47]. Because of the physicochemical properties of clinoptilolite, obtaining a catalyst that is based on this zeolite requires two- or three-step modification, such as ion-exchange and calcination. It was found that, upon ion-exchange with NH₄⁺ and thermal treatment, the zeolite did not suffer from structural degradation [47]. Clinoptilolite found its use in practical applications, especially as an adsorbent for heavy metals [48,49] or an agent utilized for groundwater remediation [50]. The presence of intermediates in the form of nitrate species, occurring during the catalytic reaction, suggested that the process proceeds according to the Langmuir-Hinshelwood mechanism. The highest conversion for the catalyst based on clinoptilolite was obtained in the temperature range of 300–450 °C. Additionally, dealumination of the zeolite with low-concentrated oxalic acid increases selectivity towards molecular nitrogen during SCR process, due to the presence of additional acidic centers [42]. Dakdareh et al. [34] studied manganese oxide nanostructures that were deposited on clinoptilolite surface and reported that propane-SCR catalytic tests that were carried out over the material indicated that the optimum activity is reached at 200 °C. It should be emphasized that most of the research over the application of modified clinoptilolite in SCR concerns the use of hydrocarbons as reducing agents and the studies over application of clinoptilolite in NH₃-SCR are very limited. One of the studies was carried out by Moreno-Tost et al. [51], who analyzed catalytic activity of Cu-exchanged clinoptilolite in oxygen-rich atmosphere and in the presence of water and SO₂. It was found that 95% conversion of NO was reached in the temperature range of 180–330 °C. Additionally, the modified clinoptilolite exhibited satisfactory tolerance to H₂O.

Thus, the aim of the present work was to verify the idea of using a new catalyst for NH₃-SCR in low- and high-temperature regions, based on modified natural zeolite. Taking the promising results of the catalytic tests obtained for protonated and/or transition metal-doped clinoptilolite into account, an attempt was made to investigate iron-modified material in NH₃-SCR. The catalyst was prepared at a laboratory scale in a powder form and, then, the series of experiments of its shaping into pellets was conducted. The activity tests were performed over the catalyst in the form of grains on a laboratory scale using a model gas mixture or the tail gases from nitric acid plant. Physicochemical studies of the catalyst (N₂ sorption at –196 °C, FT-IR, XRD, UV-vis) were performed to determine its textural structural properties and identify the surface functional groups.

2. Results and Discussion

2.1. Specific Surface Area and Textural Properties

Table 1 presents the results of the specific surface area (S_{BET}) and porosity analysis performed on the samples. The specific surface area of non-modified clinoptilolite was $14 \text{ m}^2 \text{ g}^{-1}$. The value is in agreement with the literature data, which report a specific surface area of clinoptilolite (regardless the origin) as $11\text{--}16 \text{ m}^2 \text{ g}^{-1}$ [52–55]. Such a low value of specific surface area of natural zeolite is due to the presence of cations (for example Na^+ , K^+ or Ca^{2+}) in the raw sample that block the pore channels and are a barrier for the entrance and diffusion of nitrogen molecules to the internal zeolite structure [52,56]. Additionally, the number of impurities, characteristic for natural aluminosilicates, especially clays and quartz, can influence the obtained result of structural properties [52]. It may be observed that the modification with HCl resulted in the increase of S_{BET} of clinoptilolite, which was probably due to the mild interaction of acid with the zeolitic structure. It was confirmed that the treatment of natural aluminosilicates with various acids results in the increase of specific surface area [57,58]. The result is correlated with decationation, dealumination, and dissolving of amorphous silica fragments that block the channels of raw zeolite. Thus, the framework of clinoptilolite was affected and new systems of pores were developed upon acid treatment. What is more, in the case of the fresh catalyst prepared at AGH University of Science and Technology (Fe-Clin-A), S_{BET} increased after deposition of iron, while, for the fresh catalyst that was prepared at Łukasiewicz Research Network-New Chemical Syntheses Institute (Ł-INS) (Fe-Clin-I), it was correspondingly lower. These results may be ascribed to the shaping procedure that was performed on Fe-Clin-I. The total pore volume did not change after protonation of the sample by HCl; nevertheless, the deposition of the active phase resulted in the increase of total pore volume of Fe-Clin-A. The unchanged distribution of pores after modification with HCl can be the result of insufficient strength of the leaching agent or the fact that the procedure was performed only once. This conclusion was drawn basing on the reports that the repeated treatment could give better results than the single treatment [52,53,59]. Fe-Clin-A exhibited over two times higher value of total pore volume (V_c) in comparison to Fe-Clin-I, which can be correlated with higher S_{BET} , a better developed structure and the fact that the material was not shaped. Similarly to V_c , the change of mesopore volume (V_m) after modification with acid is negligible in comparison to the raw material. The share of mesopores in Fe-Clin-A has almost doubled in relation to Fe-Clin-I. The effect of the increase of total (and mesopore) volume after deposition of the active phase can be ascribed to the interaction of the zeolite structure with the precursors of iron during precipitation, the removal of the exchangeable cations of clinoptilolite, and penetration by the escaping gases upon calcination [52,59].

Table 1. Specific surface area (S_{BET}), total pore volume (V_c), and mesopore volume (V_m) of the analyzed samples obtained from adsorption/desorption nitrogen measurements at $-196 \text{ }^\circ\text{C}$.

No.	Sample Code	S_{BET} ($\text{m}^2 \text{ g}^{-1}$)	V_c ($\text{cm}^3 \text{ g}^{-1}$)	V_m ($\text{cm}^3 \text{ g}^{-1}$)
1	Clin-non modified	14	0.062	0.033
2	H-Clin	27	0.062	0.035
3	Fe-Clin-A	37	0.137	0.079
4	Fe-Clin-I	20	0.057	0.037

2.2. X-ray Diffraction Analysis

Figure 1 presents the XRD patterns of raw clinoptilolite (Clin-non-modified), protonated form of clinoptilolite prepared at AGH (H-Clin), fresh catalysts prepared at AGH (Fe-Clin-A) and at Ł-INS (Fe-Clin-I). Figure 2 presents the comparison of the diffractograms obtained for the catalysts before and after NH_3 -SCR. The reflection maxima on the pattern of non-modified zeolite, located at $2\theta \sim 9.85, 11.18, 12.95, 19.05, 22.40, 27.95, 30.16, 31.88, 32.67, 33.62, 35.35,$ and 36.90° confirm that the main crystalline phase of the sample is clinoptilolite [29,51]. The maxima are highlighted on the pattern by their respective Miller

indices. Additionally, there are also reflections at $2\theta \sim 26.68^\circ$ and 21.87° {00-011-0695}, indicating the presence of quartz and cristobalite impurities, respectively [29]. Transformation into protonated form did not significantly influence the crystalline structure of the zeolite, since only a negligible decrease in the intensity of the diffraction maxima can be observed. Moreover, none of the characteristic diffraction maxima for iron oxide phase were detected in both of the samples modified with Fe. Thus, either the active phase was well-dispersed on the support or no crystalline phases of Fe have been formed. Nevertheless, after the modification of clinoptilolite with iron, the intensity of the diffraction maxima decreased in the case of both of the Fe-modified samples. Additionally, the reflections of cristobalite disappeared, probably due to its dissolution in the strongly acidic medium, during the synthesis procedure of Fe-modified clinoptilolite. However, the reflections of stilbite and SiO_2 remained unchanged. After the active phase deposition, the degree of crystallinity of the materials decreased. The crystallinity decrease was probably caused by the calcination and partial amorphization of the zeolite. It should be noted that the clinoptilolite framework was not damaged upon the catalytic reaction, as evidenced by the characteristic reflections that were present on the patterns of the spent catalysts.

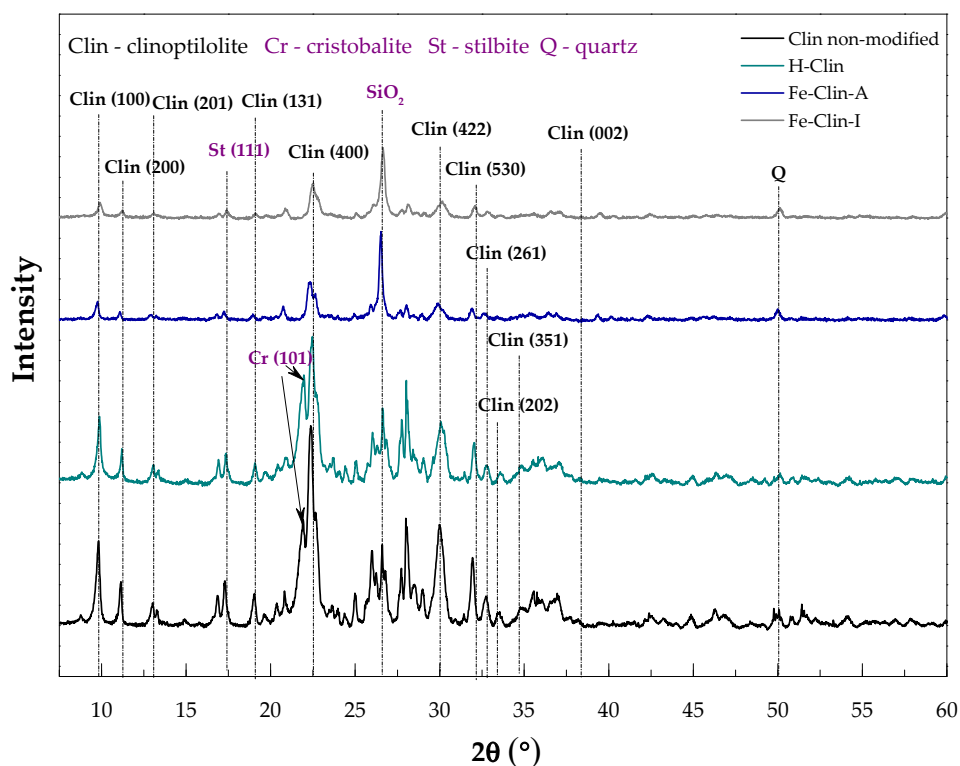


Figure 1. X-ray diffraction method (XRD) patterns of non-modified clinoptilolite, protonated form of clinoptilolite prepared at AGH (H-Clin), clinoptilolite modified with iron (Fe-Clin-A, Fe-Clin-I).

The average sizes of zeolite crystallites were calculated using Scherrer's Equation (7), and are presented in Table 2. It may be noticed that the performed modifications led to the increase of the size of clinoptilolite crystallites and Fe-Clin-I exhibited slightly bigger crystallites than Fe-Clin-A. After NH_3 -SCR, the crystallite size was higher, which suggests that their dimensions increase during the catalytic process. According to Zhang et al. [60], who studied the influence of the zeolite crystal size on the catalytic performance, larger crystallites sizes reduce the lifetime of the catalysts and its selectivity to the desired products. Therefore, the lower NO conversion obtained above 325°C for both Fe-Clin-A and Fe-Clin-I could be a result of the crystal growth. Furthermore, the presence of larger crystallites is associated with the lower specific surface area and longer residence time of

the reactants in the zeolite channels. Consequently, more by-products of the SCR reaction are formed and the selectivity of the catalyst decreases.

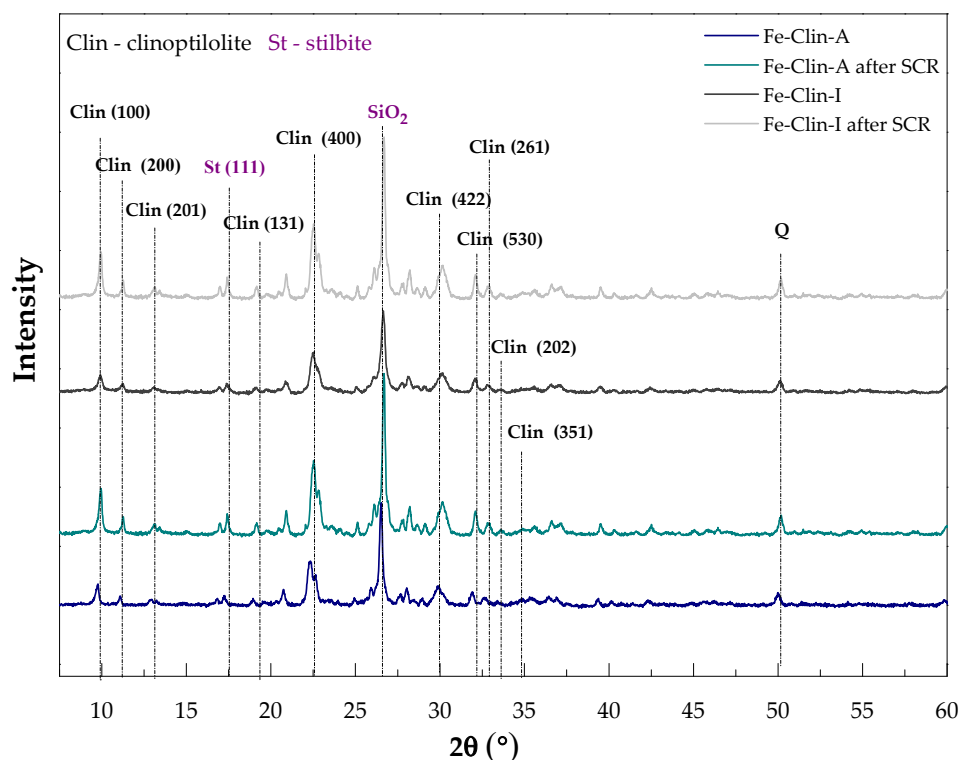


Figure 2. Comparison of XRD patterns of the Fe-Clin-A and Fe-Clin-I obtained before and after NH_3 -selective catalytic reduction (SCR) catalytic tests.

Table 2. Sizes of clinoptilolite crystallites before and after modification with iron calculated according to the Scherrer's equation.

No.	Peak Position 2θ (°)	Miller's Indices	Crystal Size of the Particular Sample (nm)				
			Clin Non-Modified	Fe-Clin-A	Fe-Clin-I	Fe-Clin-A after SCR	Fe-Clin-I after SCR
1	9.85	1 0 0	1.19	2.16	2.68	3.62	3.74
2	11.18	2 0 0	1.17	2.12	3.25	4.29	5.90
3	12.95	2 0 1	0.98	0.99	2.13	3.04	2.68
4	19.05	1 3 1	1.15	1.75	2.76	1.40	3.58
5	22.40	4 0 0	0.71	1.14	1.32	2.02	1.83
6	27.95	0 0 2	1.14	2.23	2.67	2.58	3.26
7	30.16	4 2 2	0.90	1.07	1.25	2.45	1.24
8	31.88	5 3 0	1.42	1.85	2.45	2.67	3.67
9	32.67	2 6 1	1.09	1.83	1.84	2.64	2.20
10	33.62	2 0 2	1.13	1.55	1.30	2.82	2.68
11	35.35	3 5 1	0.82	0.54	0.42	1.45	0.61
12	36.90	4 4 1	0.39	0.19	0.23	0.23	0.47
Average crystalite size (nm)			1.01	1.45	1.86	2.31	2.66

2.3. Fourier Transform Infrared Spectroscopy Analysis

Figure 3 presents the FT-IR spectra of the analyzed samples. The spectra can be divided into three wavelength ranges: O-H stretching vibrations ($3800\text{--}3400\text{ cm}^{-1}$) (1), Si-O stretching vibrations, Al-Me-OH bending vibrations, and O-H bending vibrations from H_2O molecules ($1700\text{--}700\text{ cm}^{-1}$) (2), and pseudo lattice vibrations ($700\text{--}450\text{ cm}^{-1}$) (3). The

spectra of raw and protonated clinoptilolite had almost identical shape, which indicated that the transformation into hydrogen form did not affect the zeolitic lattice. When considering the first of the mentioned regions, the band at 3635 cm^{-1} , present in the spectra of raw and protonated clinoptilolite, is assigned to the bridging OH groups vibrations in $\equiv\text{Al-OH-Si}\equiv$ and it corresponds to the location of hydrogen atoms in the vicinity of oxygen atoms in the aluminosilicate framework. For Fe-Clin-A the vibrational band is less intense, while, for Fe-Clin-I, it is similar to that obtained for non-modified clinoptilolite and H-Clin. It suggests the formation of more vibrational structures on Fe-Clin-A after the introduction of iron. The $\equiv\text{Si-OH}$ and $\equiv\text{Al-OH}$ groups are the active sites of zeolite, which provide ion-exchange properties and surface complexation that occurs during the addition or removal of hydrogen atom. Upon the synthesis of the catalyst, surface groups of clinoptilolite become negatively charged due to the loss of hydrogen ions, already present in the raw zeolite or introduced during protonation Equations (4) and (5) [61]:

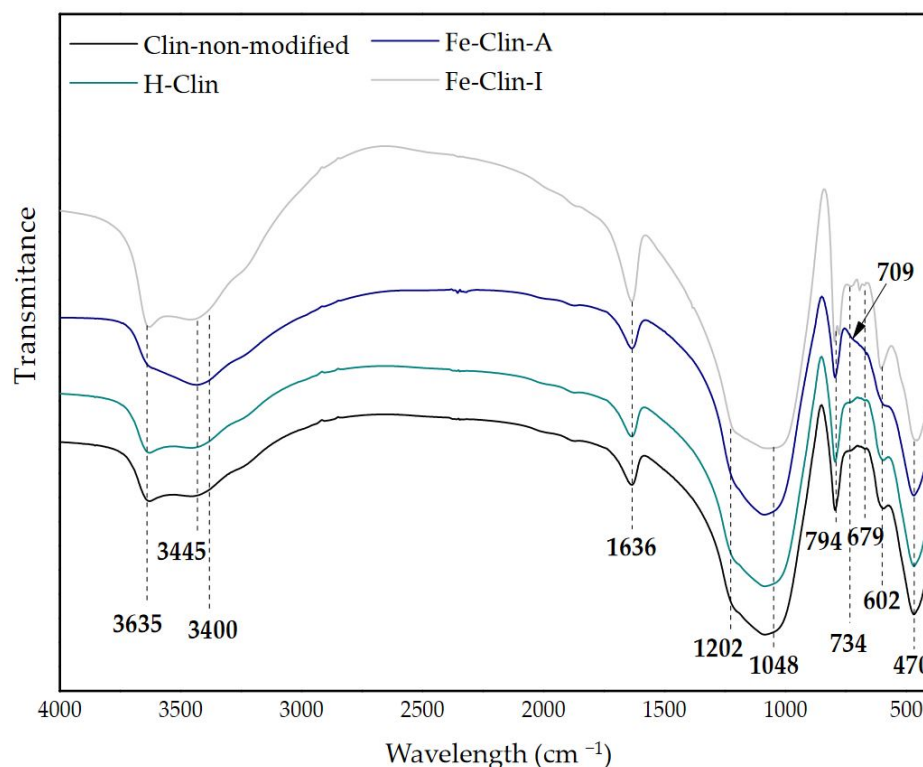
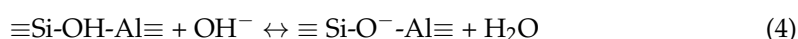


Figure 3. Fourier-Transform Infrared spectroscopy (FT-IR) spectra of non-modified clinoptilolite, H-Clin, Fe-Clin-A, and Fe-Clin-I.

Fe^{3+} cations can occupy the negatively charged active sites of the zeolite, thus, after the introduction of iron the band at 3635 cm^{-1} was significantly less sharp and the change can only be observed for this sample. It may suggest that upon co-precipitation procedure some of OH groups from $\equiv\text{Al-OH-Si}\equiv$ were affected. On the other hand, after shaping the band was somehow reconstructed, which points at the fact that the presence of OH groups was dependent on the modification procedure of the catalyst. The peak at 3445 cm^{-1} is related to the structures that arise from monomeric hydrogen bonds. This peak is slightly shifted for Fe-Clin-A toward lower frequency (3400 cm^{-1}), which points at the increased amount of hydrogen bonding in the sample [62]. In the second region, the sharp peak that is present at 1636 cm^{-1} , appearing for all of the samples, is assigned to the bending vibrations of

interlayer water molecules [29]. The peaks at 1202 cm^{-1} and 1048 cm^{-1} , identical for both modified and non-modified clinoptilolite, are attributed to Fe-O asymmetric stretching vibrations in tetrahedral FeO_4 groups, and asymmetric O-Me-O stretching vibrations (where Me = Si or Al), respectively [62,63]. The O-Me-O stretching vibration is sensitive to the content of framework silicon and aluminum [64]. Therefore, since the peak remains unchanged for non-modified and modified clinoptilolite, the performed modifications did not result in the dissolution of Si or Al. Moreover, the appearance of Fe-containing groups suggests the presence of iron species in non-modified clinoptilolite. The intense peak at 794 cm^{-1} that is observed for all of the samples confirms the presence of symmetric O-T-O stretching vibrations [62]. In the third region, the bands at 734 cm^{-1} and 679 cm^{-1} , visible only for raw and protonated clinoptilolite, are assigned to bending bonds of MeO_4 [62]. The peaks are replaced in clinoptilolite modified with iron by the broad band at 709 cm^{-1} , which indicates some structural changes in the zeolite structure. The peaks at 602 cm^{-1} and 470 cm^{-1} in the pseudo lattice vibrations region, appearing for both modified and non-modified clinoptilolite, confirm the presence of O-Me-O and internal MeO_4 bending vibrations, respectively [63].

2.4. UV-Vis Analysis

Figure 4 presents the UV-vis spectra obtained for the raw, protonated, and iron-modified clinoptilolite. Generally, there are three wavelength ranges that are expected for iron-containing materials: (1) below 300 nm for isolated Fe^{3+} sites, (2) between 300 and 400 nm for octahedral Fe^{3+} in small oligomeric Fe_2O_3 clusters, and (3) above 450 nm for large particles of Fe_2O_3 [65]. Raw clinoptilolite exhibited three bands: at 260, 370, and 495 nm. The first band is assigned to the charge transfer of oxygen to Fe^{3+} cations in octahedral coordination, while the second is due to the presence of extra-framework FeO_x oligomers. The band at 495 nm occurs due to the appearance of large Fe_2O_3 particles on the zeolite surface or oxygen-to-metal charge transfer transitions that involve octahedral Fe^{3+} species [66,67]. Clear bands that are detected for raw clinoptilolite point at the fact that iron is present in the raw material, in agreement with FT-IR analysis. After the protonation procedure, the shape of the spectra significantly changed, since the band at 495 nm disappeared completely, while the one at 370 nm was shifted to 338 nm. The band at 338 nm is due to the presence of Fe^{3+} in octahedral coordination, thus hydrogenation results in the removal of FeO_x oligomers and formation of octahedral Fe^{3+} species [66]. Nevertheless, because acid treatment did not remove iron from the raw carrier, some amount of the active phase was already present in clinoptilolite that was subjected to further modifications. The peaks in the spectra of Fe-Clin-A and Fe-Clin-I appeared in the same position of 260 nm, while an additional band at 495 nm was detected for Fe-Clin-A. Hence, the shaping of the catalyst led to the removal of bulky Fe_2O_3 larger aggregates from the surface of iron-modified clinoptilolite. The experiments that were performed by Kumar et al. [65] implied that mononuclear Fe species play the important role in NH_3 -SCR reaction. Thus, probably due to that reconstruction of the active phase during shaping, the catalytic activity of the material did not decrease. According to the literature, tetrahedrally coordinated Fe^{3+} can be detected at of 215 and 241 nm [65], and the peak at 260 nm indicates the presence of octahedral Fe^{3+} . Therefore, the modification of clinoptilolite with iron led to the increase of the number of coordinating oxygen ligands. Nevertheless, a higher intensity of the band at 495 nm in comparison to that obtained for non-modified clinoptilolite and H-Clin suggests that the iron deposition resulted in an increased amount of larger Fe_2O_3 particles [65]. However, a reliable identification of various iron species on the surface of clinoptilolite and their amount is not straightforward due to the limited sensitivity of UV-vis technique.

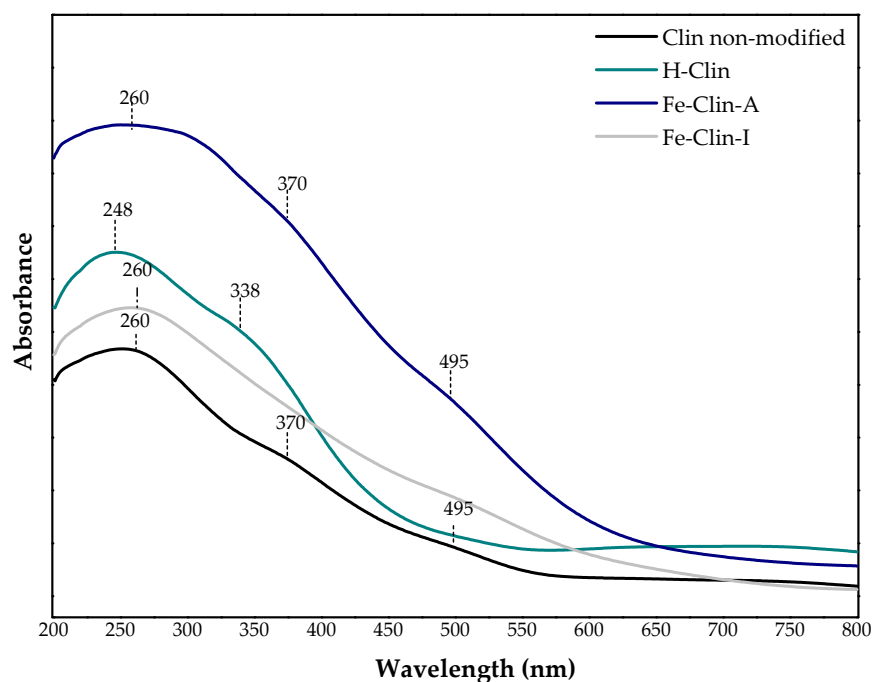


Figure 4. UV-vis spectra of non-modified clinoptilolite, H-Clin, Fe-Clin-A, and Fe-Clin-I.

2.5. Catalytic Tests

2.5.1. NH_3 -SCR Catalytic Tests Performed with Model Gas Mixture

Figures 5 and 6 present the results of NO_x catalytic tests that were obtained for non-modified clinoptilolite and both samples of clinoptilolite modified with iron. The catalytic tests were carried out with the application of a model mixture at a constant gas hourly space velocity (GHSV) of $26,500 \text{ h}^{-1}$. The obtained outcomes suggested that non-modified clinoptilolite has very high potential to act as a beneficial support of the novel NH_3 -SCR catalyst, since 58% of NO conversion was reached at 450°C . It is probably due to the presence of Fe_xO_y in the raw zeolite, as confirmed by FT-IR and UV-vis spectroscopy. The introduction of the additional amount of iron in the form of active phase elevated catalytic activity of the material, as may be observed in Figure 5. Nevertheless, the shaping of the powder catalyst resulted in the shift of the temperature of 50% conversion (t_{50}) from 225°C for Fe-Clin-A to 325°C for Fe-Clin-I. It can be observed that, in comparison to Fe-Clin-I, Fe-Clin-A exhibits significantly higher activity above 280°C . It can be caused by a lower amount of iron in the less active sample and shaping procedure that visibly affected the catalytic performance. Additionally, according to UV-vis results, the sample Fe-Clin-A does not contain more aggregated iron oxide species that give rise to the catalytic activity in the temperature range above $250\text{--}300^\circ\text{C}$ [68]. Additionally, below 350°C , NO conversion that is obtained for Fe-Clin-I is much lower than that for Fe-Clin-A. It is probably related to the shaping process performed on the catalyst. Alternatively, it can be the result of the application of a different acid during the hydrogenation step in the case of Fe-Clin-I. The difference in NO conversion obtained for these samples was lower above 400°C , since, in both cases, similar activity of 98% and 95% was obtained for the Fe-Clin-A and Fe-Clin-I, respectively. Additionally, during the experiments, N_2O concentration was measured and Figure 6 presents the obtained results. The concentration of the by-product during the experiment performed over non-modified clinoptilolite was maintained at a constant level in temperature range of $150\text{--}300^\circ\text{C}$ and, above this region, it slightly increased from around 20 ppm to 40 ppm. Similarly, for both Fe-Clin-A and Fe-Clin-I, N_2O concentration increased with the increasing temperature. However, in comparison to Fe-Clin-A, a lower amount of N_2O was obtained for Fe-Clin-I in the whole temperature range.

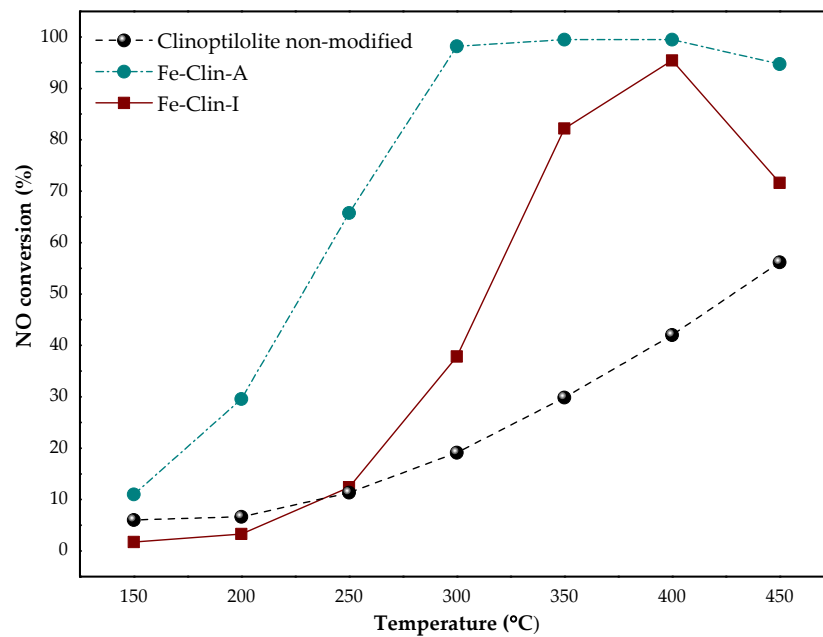


Figure 5. The results of NO conversion during NH_3 -SCR process obtained for non-modified clinoptilolite, Fe-Clin-A, and Fe-Clin-I at gas hourly space velocity (GHSV) = $26,500 \text{ h}^{-1}$.

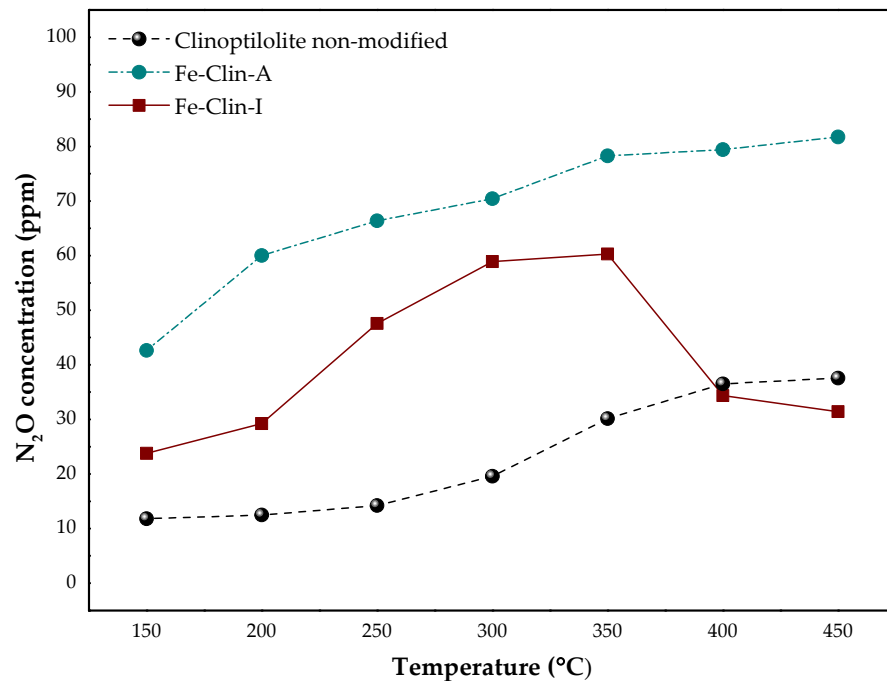


Figure 6. The results of N_2O concentration during NH_3 -SCR process obtained for non-modified clinoptilolite, Fe-Clin-A, and Fe-Clin-I at GHSV = $26,500 \text{ h}^{-1}$.

2.5.2. NH_3 -SCR Catalytic Tests Performed with Industrial Gas Mixture

The clinoptilolite-based catalyst sample was tested in the conditions that reflect those in the industrial nitric acid plant in order to provide a more comprehensive view of the catalytic performance. The experiment was performed with the tail gas from the pilot nitric acid plant of the following compositions (approximate composition): 700, 1500, 2300, 2500 ppm of NO_x , 1000–1200 of ppm N_2O , 1.0–4.0% vol. O_2 , 0.3–0.5 vol.% H_2O , in the temperature range of 250–450 °C, and GHSV = $26,500 \text{ h}^{-1}$. Figure 7 shows the course of the experiments. During the reaction, the amount of ammonia that was used for NO_x

reduction was increased and, then, the gas composition downstream of the catalytic bed was analyzed. In each case, the maximum conversion that can be obtained under the specific conditions with the minimum NH_3 slip of less than 10 ppm was calculated using Equations (9) and (10). The results that are shown in Figure 7 indicated that the analyzed catalyst is highly active in NH_3 -SCR process in the industry-reflecting conditions, since a significant decrease in NO and NO_2 concentration was observed.

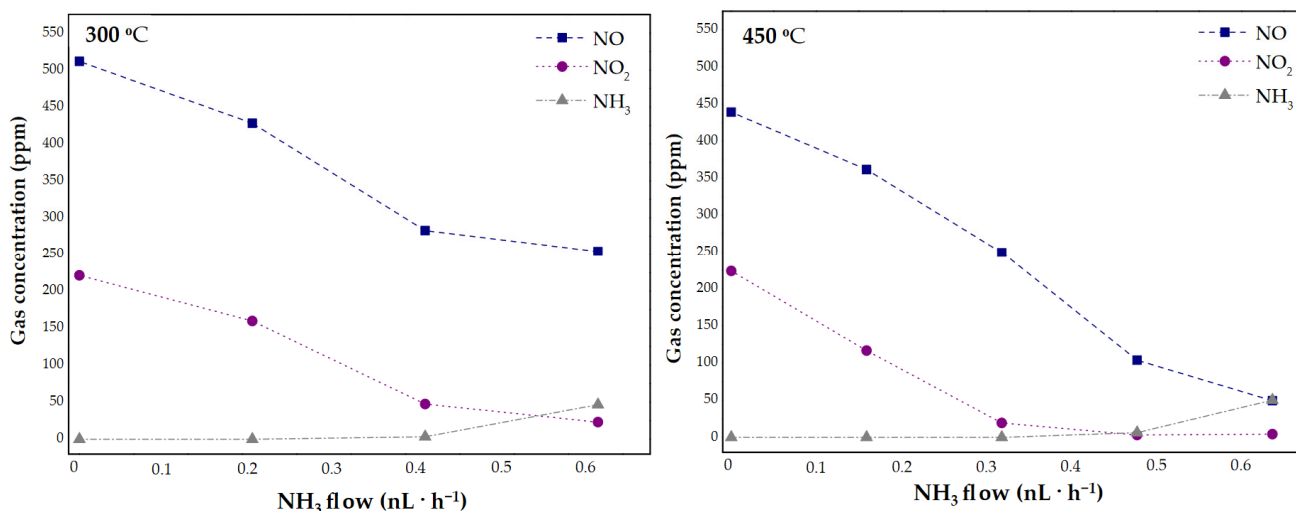


Figure 7. NO, NO_2 , and NH_3 concentration as a function of NH_3 concentration at 300 °C or 450 °C for the Fe-Clin-I at $\text{GHSV} = 26,500 \text{ h}^{-1}$.

In Figure 8, the results of the catalytic tests for different initial NO_x concentrations ($C_{\text{inlet}}(\text{NO}_x) = 700, 1500, 2300 \text{ ppm}$) are presented. As expected in all cases, NO_x conversion increased with the increasing temperature. Nevertheless, for technical reasons, it was not possible to verify the activity of the materials above 450 °C.

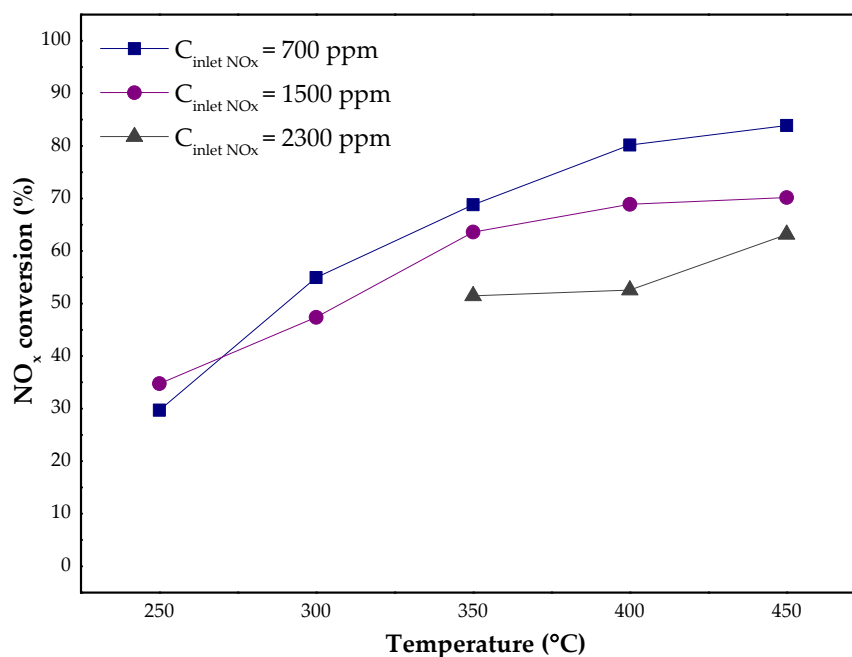


Figure 8. The results of NO_x conversion and N_2O concentration as a function of temperature and NO_x inlet concentration for the Fe-Clin-I at $\text{GHSV} = 26,500 \text{ h}^{-1}$, $C_{\text{inlet}}(\text{NO}_x) = 700, 1500, 2300 \text{ ppm}$.

The inlet concentration of NO_x in the tail gases has a significant impact on the conversion, especially at higher temperature. For the studied GHSV, the lower the inlet NO_x concentration, the higher the NO_x conversion was obtained in a specific temperature. Figure 9 presents the ratio of N_2O concentration in the outlet and inlet of the reactor. Regardless of the temperature and the inlet NO_x concentration, the ratio of the N_2O concentration downstream and upstream of the catalytic bed was lower than 1. Thus, N_2O concentration measured downstream of catalytic bed was lower than the inlet N_2O concentration. Below 350 °C, N_2O concentration was constant, or it increased slightly with the increase of NH_3 amount. The highest activity and selectivity of the catalyst in the presence of NH_3 is observed at 450 °C. Under these conditions, the amount of N_2O decreased by almost 40 ppm in comparison to its initial concentration. Therefore, it can be assumed that the studied catalyst is active not only in DeNO_x , but also in DeN_2O process.

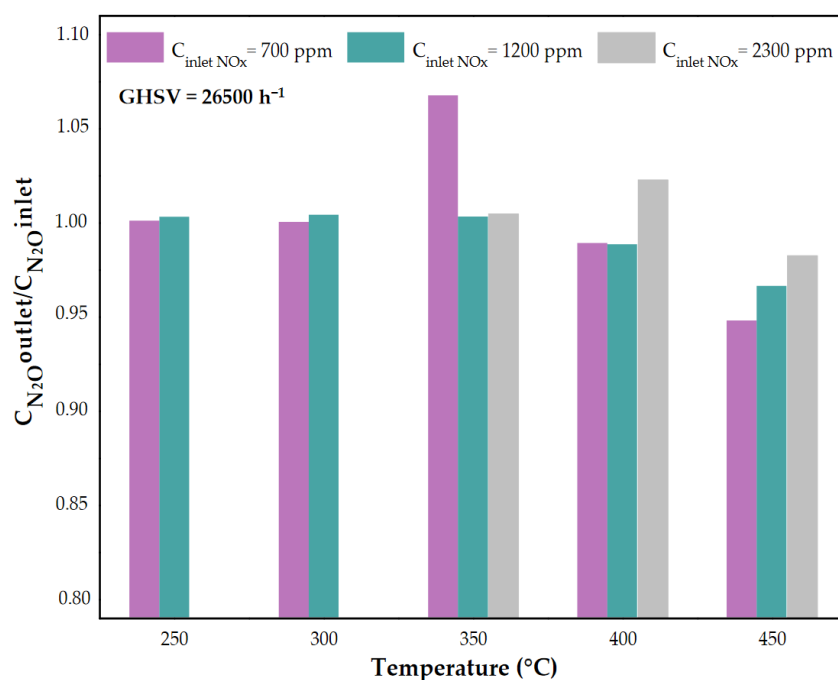


Figure 9. The ratio of N_2O concentration downstream of the catalytic bed and N_2O inlet concentration as a function of the temperature for Fe-Clin-I at $\text{GHSV} = 26,500 \text{ h}^{-1}$, $C_{\text{inlet}}(\text{NO}_x) = 700, 1500, 2300$ ppm.

Table 3 summarizes the conversion of NO and NO_2 (and the total NO_x conversion), N_2O concentration at the reactor outlet, and the ratio of N_2O concentration downstream of the catalytic bed to inlet N_2O concentration for the various operation temperatures, the constant $\text{GHSV} = 26,500 \text{ h}^{-1}$ and $C_{\text{inlet}}(\text{NO}_x) = 700$ ppm. The conversion of NO , NO_2 , and NO_x was calculated using Equations (9) and (10). The obtained results clearly indicate that, during the reduction process carried out in the variable temperature mode, the rate of NO_2 reduction is higher than the rate of NO reduction.

Table 3. NO , NO_2 , total NO_x conversion (X) and N_2O concentrations obtained for Fe-Clin-I.

Temperature (°C)	X_{NO} (%)	X_{NO_2} (%)	X_{NO_x} (%)	$C_{\text{N}_2\text{O outlet}}$ (ppm)	$C_{\text{N}_2\text{O outlet}}/C_{\text{N}_2\text{O inlet}}$ (-)
250	22.9	44.2	29.7	1028	1.00
300	44.7	78.5	54.9	1025	1.00
350	56.7	95.7	68.8	1195	1.07
400	71.0	98.1	80.2	1216	0.99
450	76.4	98.6	83.9	1156	0.95

The results of NH_3 -SCR experiments in the flow of the tail gas stream showed that achieving a satisfactory conversion of NO_x below 300°C is not possible for the catalyst loading comparable to that of an industrial catalytic bed. The highest NO_x reduction (over 80%) was obtained at 400°C and, interestingly, above this temperature simultaneous N_2O decomposition was observed (even several percent N_2O conversion). Therefore, in the next step of the studies, NH_3 -SCR experiments were performed at 450°C .

The results of NO_x conversion versus GHSV at 450°C and the ratio of N_2O concentration downstream of the catalytic bed to that at the reactor inlet at 450°C versus GHSV are shown in Figures 10 and 11, respectively.

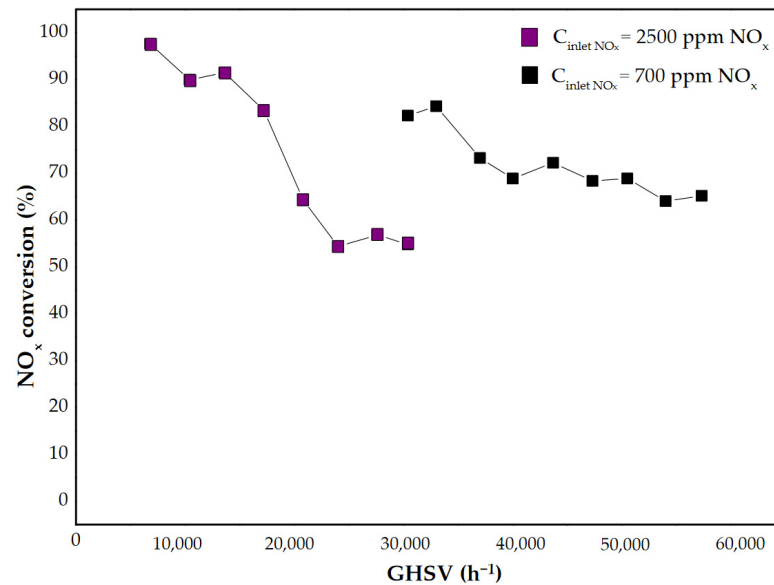


Figure 10. The results of NO_x conversion as a function of GHSV for the shaped Fe-Clin-I catalyst sample at 450°C .

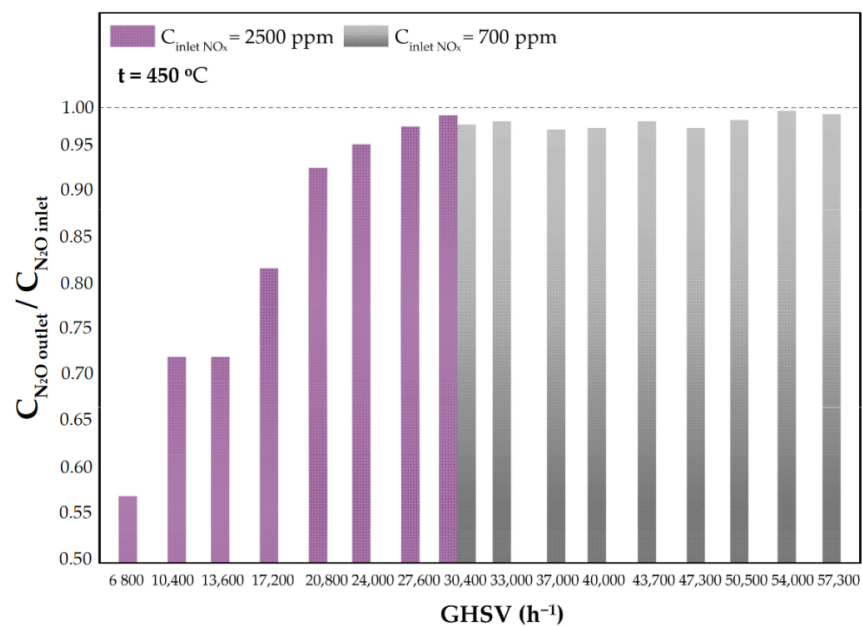
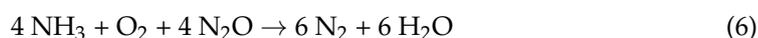


Figure 11. The ratio of the N_2O concentration at the reactor outlet to the inlet N_2O concentration as a function of GHSV for the Fe-Clin-I shaped catalyst sample at 450°C and $C_{inlet}(\text{NO}_x) = 2500$ ppm and $C_{inlet}(\text{NO}_x) = 700$ ppm.

In Figure 10 the results of NO_x conversion are presented as a function of GHSV for two significant values of the inlet NO_x concentrations, which are $C_{inlet}(\text{NO}_x) = 700$ ppm and $C_{inlet}(\text{NO}_x) = 2500$ ppm, respectively. As expected, NO_x conversion decreased with the increase of the catalyst load. Moreover, a higher NO_x conversion was obtained for a lower inlet NO_x concentration. The performed research also showed the beneficial influence of the catalyst on N₂O concentration in the gas mixture—it contributes to the decrease of N₂O emission downstream of the reactor, as shown in Figure 11. At 450 °C, the N₂O concentration measured downstream of the catalytic bed was lower than the inlet N₂O concentration. It was observed that the NO_x inlet concentration does not substantially affect the degree of N₂O decomposition/reduction. Moreover, regardless of the inlet concentration of NO_x, a similar ratio of $C_{\text{N}_2\text{O outlet}}/C_{\text{N}_2\text{O inlet}}$ was obtained at GHSV = 30,400 h⁻¹, as shown in Figure 11.

It indicated that, above 400 °C, N₂O decomposition takes place or the N₂O reduction reaction starts at the catalyst surface according to Equation (6) [4]:



2.6. Materials and Methods

2.6.1. Catalysts Preparation

The preparation of the studied catalysts was performed at the laboratory of AGH and at Ł-INS. The obtained catalysts were labeled as Fe-Clin-A and Fe-Clin-I, respectively. Table 4 lists all of the prepared and analyzed samples.

Table 4. The list of the studied samples with their codes and descriptions.

Sample Code	Description of the Sample
Clin-non modified	Clinoptilolite before modifications
H-Clin	Protonated form of clinoptilolite prepared at AGH
Fe-Clin-A	H-Clin with iron deposited via precipitation procedure
Fe-Clin-A after SCR	Fe-Clin-A after catalytic reaction
Fe-Clin-I	H-Clin with iron deposited via precipitation procedure shaped into tablets
Fe-Clin-I after SCR	Fe-Clin-I after catalytic reaction

Raw clinoptilolite was transformed into a hydrogen form by two hours-lasting ion-exchange with 5 vol.% solution of HCl, repeated three times, in order to prepare Fe-Clin-A. The mass ratio of the zeolite to the acid was 1:3. Afterwards, the material was dried at 80 °C overnight. The support was subsequently modified with iron by precipitation method. H-clinoptilolite was added to 0.05 M solution of FeSO₄ and vigorously stirred at 50 °C for 4 h, maintaining pH around 3.0. Next, the pH of the mixture was increased to 9.0 using 25 vol.% aqueous solution of NH₃, added dropwise. The alkaline suspension was stirred for another one hour. The modified zeolite was filtered and washed several times with distilled water to remove the majority of residual ammonia from its surface. The obtained material was dried at 80 °C overnight and calcined at 450 °C for two hours.

Fe-Clin-I was prepared according to the procedure similar to Fe-Clin-A and it was then shaped into pellets. The only difference in the synthesis method of Fe-Clin-A and Fe-Clin-I materials was the application of HNO₃ instead of HCl in the stage of protonation. We speculate that the usage of different acid did not significantly change the catalytic properties of Fe-modified clinoptilolite in the temperature range that we are interested in. After calcination, the resulting catalyst was homogenized and shaped into pellets, while using a laboratory pellet press. The dimensions of the pellets were 5 mm (diameter) × 4.8 mm (height) and their bulk density was in the range of 1.3–1.4 g cm⁻³. Figure 12 presents the obtained pellets.



Figure 12. Fe-Clin-I shaped into pellets.

2.6.2. Catalysts Characterization

The following parameters were determined:

- the specific surface area, total pore volume and mesopore volume were calculated from low-temperature N₂ sorption isotherm (−196 °C, $p/p_0 \leq 0.99$, BET (Brunauer–Emmett–Teller) adsorption model and BJH (Barret–Joyner–Halenda) transformation for mesopores characteristics), equipment: ASAP[®] 2050 Xtended Pressure sorption analyzer (Micromeritics Instrument Co., Norcross, GA, USA);
- the crystallographic structure by the X-ray diffraction method (XRD) (Cu-K α LFF HR, $\lambda = 1.54059 \text{ \AA}$; 2θ range 2.0–40.0°; step 0.02°; 1 s/step), equipment: Empyrean diffractometer (Panalytical, Almelo, Netherlands); the average size of crystallites was calculated using Scherrer's formula (7):

$$D_{hkl} = \frac{K\lambda}{\beta_{hkl} \cos \theta'} \quad (7)$$

- the characteristic chemical groups by Fourier-Transform Infrared spectroscopy (FT-IR): wavelength range: 4000–400 cm^{−1}, resolution 4 cm^{−1}; sample was mixed with KBr into disk, ratio = 1:100; equipment: Frontier FT-IR (Perkin Elmer, Waltham, MA, USA); and,
- the coordination and aggregation of iron species from UV-Vis spectroscopy; the wavelength range 200–900 nm, resolution 1 nm; equipment: Lambda 35 UV-Vis Spectrophotometer (Perkin Elmer, Waltham, MA, USA).

2.6.3. Catalytic Tests

NH₃-SCR catalytic tests for all of the catalyst samples in the powdered form and in model gas stream were performed at AGH University of Science and Technology (AGH) at the atmospheric pressure. The reaction mixture contained 800 ppm of NO, 800 ppm of NH₃, 3.5 vol.% of O₂ and balance He, to maintain the total flow throughout the catalytic bed close to 100 cm³ min^{−1}. The catalyst sample of 0.2 g with the grain size between 0.4 and 1.0 mm was introduced to the fix-bed flow microreactor. The activity tests were carried out in the temperature ramps of 150, 200, 250, 300, 350, 400, and 450 °C (temperature increase rate 10 °C min^{−1}). The catalyst was kept at each temperature for 30 min. The temperature inside the reactor was controlled by the thermocouple installed near the central part of the catalytic bed. The concentrations of non-reacted NO and N₂O as a by-product were analyzed downstream of the reactor by FT-IR detector (ABB 2000 AO, Frankfurt, Germany). NO conversion was calculated according to Equation (8):

$$X_{\text{NO}} = \frac{\text{NO}_{in} - \text{NO}_{out}}{\text{NO}_{in}} \cdot 100\%, \quad (8)$$

It should be emphasized that the experiments performed with the model gas mixture only show the catalyst behavior in the kinetic regime and they do not provide extended information about the performance of the catalyst in the industry-reflecting conditions. Because of that, the influence of gaseous components, such as NO_2 , N_2O , and H_2O , on the catalytic performance of the material cannot be observed. Therefore, some of the experiments were conducted with the application of GHSV similar the industrial one, thus, in the diffusion-kinetic regime. The samples of the catalysts were shaped into pellets and tested in a laboratory installation at L-INS in the flow of the tail gas stream that was taken from the pilot ammonia oxidation plant. The composition of the mixture is similar to that of the tail gas emitted from industrial nitric acid plants and contains NO , NO_2 , N_2O , O_2 , N_2 , and H_2O . The laboratory installation consists of heat exchanger (HEX) for the tail gas pre-heating and a reactor (R) with a diameter of $d = 25$ mm, equipped with a heating mantle and a temperature control unit. Figure 13 shows the schematic representation of the installation. The tail gas, before entering the catalytic bed, was mixed with ammonia heated in the heat exchanger (HEX_{NH_3}).

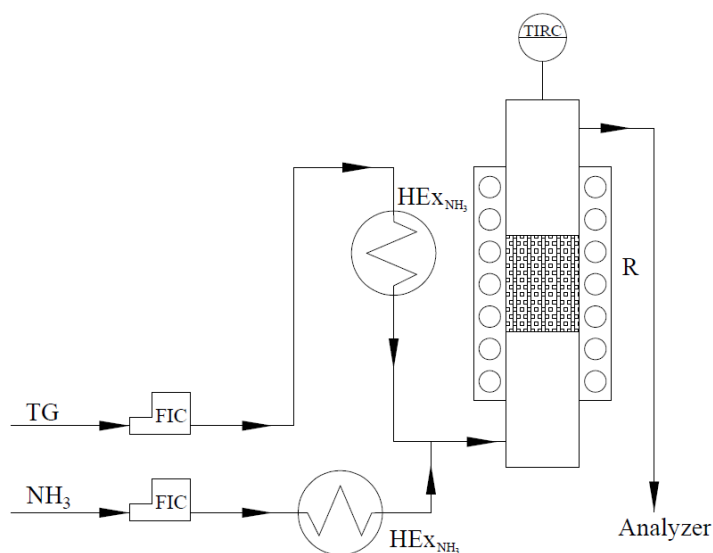


Figure 13. The scheme of the laboratory installation for NH_3 -SCR catalytic tests performed over Fe-Clin-I.

In the case of catalytic tests performed at L-INS, 22 g of the catalysts was used, and the experiments were carried out at the temperature ramps of 250, 300, 350, 400, and 450 °C. The measurements of the inlet and outlet concentrations of NO , NO_2 , N_2O , and NH_3 were performed at each temperature after the equilibrium conditions and operating parameters were stabilized. The composition of the mixture was as follows (approximate composition): 700, 1500, 2300, and 2500 ppm of NO_x , NH_3 in the amount necessary to achieve maximum NO_x conversion without ammonia slip in the gas stream, 1.0–4.0 vol.% of O_2 , around 700–1200 ppm N_2O , less than 0.5 vol.% of H_2O , and N_2 . The tests were performed at GHSV in the range of 7000–57,000 h^{-1} . The concentrations of non-reacted NO , NO_2 , and N_2O were analyzed downstream of the reactor by FT-IR GASMET analyzer (Vantaa, Finland). NO and NO_2 and the total NO_x conversion was calculated according to Equations (8)–(10), respectively:

$$X_{\text{NO}_2} = \frac{\text{NO}_2 \text{ in} - \text{NO}_2 \text{ out}}{\text{NO}_2 \text{ in}} \cdot 100\% \quad (9)$$

$$X_{\text{NO}_x} = \frac{\text{NO}_x \text{ in} - \text{NO}_x \text{ out}}{\text{NO}_x \text{ in}} \cdot 100\% \quad (10)$$

The conversion under the specific conditions was defined as the maximum conversion that can be obtained under these conditions (temperature and load, initial NO_x concentration) with the minimum NH₃ slip (NH₃ concentration at the reactor outlet <10 ppm).

3. Conclusions

In the present study, the catalytic potential of iron-modified clinoptilolite in NH₃-SCR in the temperature range of 150–450 °C was examined.

XRD analysis of the powder and shaped catalysts indicated that iron oxide was highly dispersed on the surface of both materials. What is more, the crystallinity of zeolite was only slightly lowered upon the catalytic reaction, which suggested that the structure of clinoptilolite is stable in the conditions of the process. The results of crystal size calculations indicated that the crystallites increase during NH₃-SCR, thus a slight decrease in catalytic activity of both samples can be explained by the aggregation of the particles of Fe_xO_y above 325 °C. The results of FT-IR and UV-vis studies confirmed that iron was present in the raw structure of clinoptilolite. It explains the relatively high catalytic activity of the raw zeolite, which is approximately 58% at 450 °C. UV-vis experiments indicated the co-existence of different iron sites on the clinoptilolite surface. It was found that, for the shaped sample, iron is mainly present in the form of isolated Fe³⁺ sites of various coordination that cannot be clearly distinguished. Nevertheless, probably due to that the catalyst preserved a high, satisfactory performance during NH₃-SCR despite the reconstruction of the form of iron species after shaping. The catalytic tests that were performed at Ł-INS were carried out to obtain a detailed view on the influence of the operation temperature in the reactor, catalyst loading, and the amount of added ammonia on the catalytic performance after the shaping procedure. Iron-modified clinoptilolite exhibited high activity above 300 °C when the model gas was used for the reaction. Under the same conditions, 82% NO conversion was obtained for previously shaped iron-doped clinoptilolite. When the catalyst loading during the tests was similar to the industrial one, the highest catalytic activity was obtained above 400 °C, maintaining very advantageous selectivity towards N₂. Additionally, N₂O formation was not observed during the catalytic reaction. What is more, with respect to its inlet concentration, even a slight decrease in the amount of nitrous oxide in the tail gas stream was detected.

Author Contributions: Conceptualization, M.S., M.M. and M.I.; Methodology, M.S., A.S. and M.I.; Resources, A.S., K.A.-J.; Investigations, M.S. and A.S.; Writing—original draft preparation, M.S. and A.S.; Writing—review and editing, M.I. and B.S.; Supervision, M.I., M.M. All authors have read and agreed to the published version of the manuscript.

Funding: M.M. and B.S. acknowledge the financial support founded by the Grant AGH 16.16.210.476. A.S. thank for funding research under Grant AGH 501.696.7996. M.S. acknowledge the financial support founded by the program of the Ministry of Science and Higher Education entitled “Implementation Doctorate”.

Conflicts of Interest: The authors declare no conflict of interest.

Abbreviations

Symbols

S_{BET}	specific surface area (m ² ·g ⁻¹)
V_c	total pore volume, determined by the Barret-Joyner-Halend method (m ³ ·g ⁻¹)
V_m	mesopore volume, determined by the Barret-Joyner-Halend method (m ³ ·g ⁻¹)
X_{NO}	NO conversion (%)
X_{NO_2}	NO ₂ conversion (%)
X_{NO_x}	NO _x conversion (%)
$C_{N_2O outlet}$	outlet concentration of N ₂ O (ppm)

$C_{N_2O\ out} / C_{N_2O\ in}$	outlet concentration of N_2O to inlet concentration of N_2O ratio (-)
D_{hkl}	average crystallite size in a direction normal to the diffracting plane (hkl) (Å)
K	constant (value close to unity, usually 0.8–0.9)
λ	wavelength of the X-ray sources (0.15406 nm)
β_{hkl}	diffraction line width at half of its height (rad)
θ	reflection position in radians
NO_{in}	inlet concentration of NO (ppm)
NO_{out}	outlet concentration of NO (ppm)
$NO_{2\ in}$	inlet concentration of NO_2 (ppm)
$NO_{2\ out}$	outlet concentration of NO_2 (ppm)
$NO_x\ in$	inlet concentration of NO_x (ppm)
$NO_x\ out$	outlet concentration of NO_x (ppm)

References

- Kamphus, M. Emission monitoring in nitric acid plants. In Proceedings of the Nitrogen+Syngas, Paris, France, 24–27 February 2014; Volume 328, pp. 48–53.
- Council Decision (EU) 2017/1757 of 17 July 2017 on the Acceptance on behalf of the European Union of an Amendment to the 1999 Protocol to the 1979 Convention on Long-Range Transboundary Air Pollution to Abate Acidification, Eutrophication and Ground-Level. *OJL* **2017**, *248*, 3–75.
- IPPC Page: Komisja Europejska; Zintegrowane Zapobieganie Zanieczyszczeniom oraz Kontrola, Dokument Referencyjny dla: najlepsze dostępne techniki dla Przemysłu Wielkotonażowych związków Nieorganicznych-Amoniaku, Kwasów i Nawozów Sztucznych. 2007. Available online: https://ippc.mos.gov.pl/ippc/custom/large%20volume%20inorganic%20chemicals_bref_0907_na%20strone.pdf (accessed on 12 February 2021).
- Kim, M.H.; Yang, K.H. The Role of Fe_2O_3 Species in Depressing the Formation of N_2O in the Selective Reduction of NO by NH_3 over V_2O_5/TiO_2 -Based Catalysts. *Catalysts* **2018**, *8*, 134.
- Gramiccioni, G.; Tran, P.; Patchett, J.; Gegan, T. AlCatalytic Article Comprosing a Coprecipitate of Vanadia, Tungsta, ang Titania 2017. Patent Number WO 216,690, 21 December 2017.
- Lee, T.; Bai, H. Low temperature selective catalytic reduction of NO_x with NH_3 over Mn-based catalyst: A review. *Environ. Sci.* **2016**, *3*, 261–289. [[CrossRef](#)]
- Due-Hansen, J. *Alternative deNOx Catalysts and Technologies*; Technical University of Denmark: Kongens Lyngby, Denmark, 2010.
- Gao, F.; Tang, X.; Yi, H.; Zhao, S.; Wang, J.; Shi, Y.; Meng, X. Novel Co– or Ni–Mn binary oxide catalysts with hydroxyl groups for NH_3 -SCR of NO_x at low temperature. *Appl. Surf. Sci.* **2018**, *443*, 103–113. [[CrossRef](#)]
- Koebel, M.; Madia, G.; Elsener, M. Selective catalytic reduction of NO and N_2O at low temperatures. *Catal. Today* **2002**, *73*, 239–247. [[CrossRef](#)]
- Willi, R. *Low-Temperature Selective Catalytic Reduction of NOx Catalytic Behavior and Kinetic Modeling*; Swiss Federal Institute of Technology Zurich: Zürich, Switzerland, 1996.
- Kwon, D.W.; Park, K.H.; Ha, H.P.; Hong, S.C. The role of molybdenum on the enhanced performance and SO_2 resistance of V/Mo-Ti catalysts for NH_3 -SCR. *Appl. Surf. Sci.* **2019**, 1167–1177. [[CrossRef](#)]
- Inger, M.; Rajewski, J.; Ruszak, M.; Wilk, M. The influence of NO_x presence on the catalytic N_2O decomposition over the supported double-promoted cobalt spinel catalyst. *Chem. Pap.* **2019**, *73*, 1979–1986. [[CrossRef](#)]
- Perbandt, C. Reducing the Emission of Nitrogen Oxide When Starting Up Systems for Producing Nitric Acid 2015. Patent Number WO 185,506, 10 December 2015.
- Granger, J.F. A1 A method and Apparatus for Removing NO_x and N_2O from a Gas 2015. European Patent EP 3,162,427, 3 May 2017.
- Marangozis, J. Comparison and analysis of intrinsic kinetics and effectiveness factors for the catalytic reduction of NO with ammonia in the presence of oxygen. *Ind. Eng. Chem.* **1992**, 987–994. [[CrossRef](#)]
- Schwefer, M.; Siefert, R.; Pinnow, S. A1 Device and Method for Eliminating NO_x and N_2O . U.S. Patent 0363359, 26 September 2014.
- Nonnenmacher, H.; Kartte, K. Selective Removal of Oxides of Nitrogen from Gas Mixtures Containing Oxygen. U.S. Patent 3,279,884, 10 October 1966.
- Nakajima, F.; Takeuchi, M.; Matsuda, S.; Uno, S.; Mori, T.; Wotanabe, Y. Catalytic Process for Reducing Nitrogen Oxides to Nitrogen. U.S. Patent 4,085,193, 18 April 1978.
- Searles, R. Pollution from Nitric Acid Plants. *Platin. Met. Rev.* **1973**, *17*, 57–63.
- Nam, I.-S.; Choo, S.; Koh, D.J.; Kim, Y.G. A pilot plant study for selective catalytic reduction of NO by NH_3 over mordenite-type zeolite catalysts. *Catal. Today* **1997**, *38*, 181–186. [[CrossRef](#)]
- Grande, C.A.; Anne Andreassen, K.; Cavka, J.H.; Waller, D.; Lorentsen, O.-A.; Øien, H.; Zander, H.-J.; Poulston, S.; García, S.; Modeshia, D. Process Intensification in Nitric Acid Plants by Catalytic Oxidation of Nitric Oxide. *Ind. Eng. Chem. Res.* **2018**, *57*, 10180–10186. [[CrossRef](#)]

22. Samojeden, B.; Grzybek, T. The influence of the promotion of N-modified activated carbon with iron on NO removal by NH₃-SCR. *Energy* **2016**, *116*, 1484–1491. [[CrossRef](#)]
23. Liu, K.; Yu, Q.; Wang, B.; Qin, Q.; Wei, M.; Fu, Q. Low temperature selective catalytic reduction of nitric oxide with urea over activated carbon supported metal oxide catalysts. *Environ. Technol.* **2020**, *41*, 808–821. [[CrossRef](#)]
24. Gholami, Z.; Luo, G. Low-Temperature Selective Catalytic Reduction of NO by CO in the Presence of O₂ over Cu:Ce Catalysts Supported by Multiwalled Carbon Nanotubes. *Ind. Eng. Chem. Res.* **2018**, *57*, 8871–8883. [[CrossRef](#)]
25. Raja, S.; Alphin, M.S. Systematic effects of Fe doping on the activity of V₂O₅/TiO₂-carbon nanotube catalyst for NH₃-SCR of NO_x. *J. Nanopart. Res.* **2020**, *22*. [[CrossRef](#)]
26. Chen, S.; Yan, Q.; Zhang, C.; Wang, Q. A novel highly active and sulfur resistant catalyst from Mn-Fe-Al layered double hydroxide for low temperature NH₃-SCR. *Catal. Today* **2019**, *327*, 81–89. [[CrossRef](#)]
27. Szymaszek, A.; Motak, M.; Samojeden, B. The application of modified layered double hydroxides in selective catalytic reduction of nitrogen oxides by ammonia (NH₃-SCR). *Polish J. Chem. Technol.* **2020**, *22*, 61–67. [[CrossRef](#)]
28. Samojeden, B.; Grzybek, T.; Kowal, J.; Szymaszek, A.; Jabłońska, M.; Glaeser, R.; Motak, M. The influence of holmium on catalytic properties of Fe or Cu-modified vermiculites. *Physicochem. Probl. Miner. Process.* **2019**, *55*, 1484–1495.
29. Szymaszek, A.; Samojeden, B.; Motak, M. Selective catalytic reduction of NO_x with ammonia (NH₃-SCR) over transition metal-based catalysts-influence of the catalysts support. *Physicochem. Probl. Miner. Process.* **2019**, *55*, 1429–1441. [[CrossRef](#)]
30. Szymaszek, A.; Kubeł, M.; Samojeden, B.; Motak, M. Modified bentonite-derived materials as catalysts for selective catalytic reduction of nitrogen oxides. *Chem. Process Eng.* **2020**, *41*, 13–24.
31. Chmielarz, L.; Wojciechowska, M.; Rutkowska, M.; Adamski, A.; Węgrzyn, A.; Kowalczyk, A.; Dudek, B.; Boroń, P.; Michalik, M.; Matusiewicz, A. Acid-activated vermiculites as catalysts of DeNO_x process. *Catal. Today* **2012**, *191*, 25–31. [[CrossRef](#)]
32. Xin, Y.; Li, Q.; Zhang, Z. Zeolitic Materials for DeNO_x Selective Catalytic Reduction. *ChemCatChem* **2018**, *10*, 29–41. [[CrossRef](#)]
33. Rutkowska, M.; Díaz, U.; Palomares, A.E.; Chmielarz, L. Cu and Fe modified derivatives of 2D MWW-type zeolites (MCM-22, ITQ-2 and MCM-36) as new catalysts for DeNO_x process. *Appl. Catal. B Environ.* **2015**, *168–169*, 531–539. [[CrossRef](#)]
34. Dakdareh, A.M.; Falamaki, C.; Ghasemian, N. Hydrothermally grown nano-manganese oxide on clinoptilolite for low-temperature propane-selective catalytic reduction of NO_x. *J. Nanopart. Res.* **2018**, *20*, 309. [[CrossRef](#)]
35. Oord, R.; Weckhuysen, B.M. Cu-Zeolite Selective Catalytic Reduction Catalysts for NO_x Conversion. *Zeolites Zeolite Like Mater.* **2016**, *10*, 433–450.
36. Macina, D.; Piwowarska, Z.; Góra-Marek, K.; Tarach, K.; Rutkowska, M.; Girman, V.; Błachowski, A.; Chmielarz, L. SBA-15 loaded with iron by various methods as catalyst for DeNO_x process. *Mater. Res. Bull.* **2016**, *78*, 72–82. [[CrossRef](#)]
37. Maurer, S.; Wycisk, M.; Petry, J.; Deuerlein, S.; Zhang, W.; Shi, C.; Takashi, H. Al Iron and Copper Containing Zeolite Beta from Organotemplate-Free Synthesis and Use Thereof in the Selective Catalytic Reduction of NO_x. U.S. Patent 0202524, 8 August 2013.
38. Paden, C.; Gao, F.; Wang, Y.; Kollar, M.; Szanyi, J. Catalysts for Enhanced Reduction of NO_x Gases and Process for Making and Using Same. U.S. Patent 0021725, 25 January 2018.
39. Andersen, P.; Doura, K. Al Method and Exhaust System for Treating NO_x in Exhaust Gas from Stationary Emission Sources. U.S. Patent 0341022, 30 November 2017.
40. Bull, I.; Muller, U. Copper Containing ZSM-34, OFF and/or ERI Zeolitic Material for Selective Reduction of NO_x. Patent Number WO 007874, 19 January 2012.
41. Schwefer, M.; Groves, M.; Perbandt, C.; Siefert, R. Al Process and Apparatus for Eliminating NO_x and N₂O. U.S. Patent 0149225, 13 January 2013.
42. Ghasemian, N.; Falamaki, C.; Kalbasi, M.; Khosravi, M. Enhancement of the catalytic performance of H-clinoptilolite in propane-SCR-NO_x process through controlled dealumination. *Chem. Eng. J.* **2014**, *252*, 112–119. [[CrossRef](#)]
43. Ambrozova, P.; Kynicky, J.; Urubek, T.; Nguyen, V.D. Synthesis and Modification of Clinoptilolite. *Molecules* **2017**, *22*, 1107. [[CrossRef](#)] [[PubMed](#)]
44. Gelves, J.F.; Dorkis, L.; Márquez, M.A.; Álvarez, A.C.; González, L.M.; Villa, A.L. Activity of an iron Colombian natural zeolite as potential geo-catalyst for NH₃-SCR of NO_x. *Catal. Today* **2019**, *320*, 112–122. [[CrossRef](#)]
45. Ramishvili, M.; Tsitsishvili, V.G.; Kokiashvili, N.G.; Gabunia, V.M.; Inanashvili, N.M. Modified Forms of Natural Zeolites–Clinoptilolite and Heulandite as an Effective Catalysts for Synthesis of Acetylsalicylic Acid. *Asian J. Sci. Technol.* **2017**, *8*, 4985–4995.
46. Roth, W.J.; Nachtigall, P.; Morris, R.E.; Čejka, J. Two-dimensional zeolites: Current status and perspectives. *Chem. Rev.* **2014**, *114*, 4807–4837. [[CrossRef](#)]
47. Ghasemian, N.; Falamaki, C.; Kalbasi, M. Clinoptilolite zeolite as a potential catalyst for propane-SCR-NO_x: Performance investigation and kinetic analysis. *Chem. Eng. J.* **2014**, *236*, 464–470. [[CrossRef](#)]
48. Li, Y.; Bai, P.; Yan, Y.; Yan, W.; Shi, W.; Xu, R. Removal of Zn²⁺, Pb²⁺, Cd²⁺, and Cu²⁺ from aqueous solution by synthetic clinoptilolite. *Microporous Mesoporous Mater.* **2019**, *273*, 203–211. [[CrossRef](#)]
49. Zanin, E.; Scapinello, J.; de Oliveira, M.; Rambo, C.L.; Franscescon, F.; Freitas, L.; de Mello, J.M.M.; Fiori, M.A.; Oliveira, J.V.; Dal Magro, J. Adsorption of heavy metals from wastewater graphic industry using clinoptilolite zeolite as adsorbent. *Process Saf. Environ. Prot.* **2017**, *105*, 194–200. [[CrossRef](#)]

50. Vocciant, M.; De Folly D'Auris, A.; Finocchi, A.; Tagliabue, M.; Bellettato, M.; Ferrucci, A.; Reverberi, A.P.; Ferro, S. Adsorption of ammonium on clinoptilolite in presence of competing cations: Investigation on groundwater remediation. *J. Clean. Prod.* **2018**, *198*, 480–487. [[CrossRef](#)]
51. Moreno-Tost, R.; Santamaría-González, J.; Rodríguez-Castellón, E.; Jiménez-López, A.; Autié, M.A.; González, E.; Glacial, M.C.; Pozas, C.D. Las Selective catalytic reduction of nitric oxide by ammonia over Cu-exchanged Cuban natural zeolites. *Appl. Catal. B Environ.* **2004**, *50*, 279–288. [[CrossRef](#)]
52. Korkkuna, O.; Leboda, R.; Skubiszewska-Zięba, J.; Vrublevs'ka, T.; Gun'ko, V.M.; Ryczkowski, J. Structural and physicochemical properties of natural zeolites: Clinoptilolite and mordenite. *Microporous Mesoporous Mater.* **2006**, *87*, 243–254. [[CrossRef](#)]
53. Hernández, M.A.; Rojas, F.; Lara, V.H. Nitrogen-sorption characterization of the microporous structure of clinoptilolite-type zeolites. *J. Porous Mater.* **2000**, *7*, 443–454. [[CrossRef](#)]
54. Vasylechko, V.O.; Gryshchouk, G.V.; Lebedynets, L.O.; Kuz'ma, Y.B.; Vasylechko, L.O.; Zakordonskiy, V.P. Adsorption of copper on Transcarpathian clinoptilolite. *Adsorpt. Sci. Technol.* **1999**, *17*, 125–134. [[CrossRef](#)]
55. Leboda, R.; Skubiszewska-Zięba, J. Badania nad przydatnością zakarpaccyego klinoptylolitu do adsorpcji chloroformu z roztworów wodnych. *Ochr. Środowiska* **1998**, *3*, 27–30.
56. Mansouri, N.; Rikhtegar, N.; Panahi, H.A.; Atami, F.; Shahraki, B.K. Porosity, characterization and structural properties of natural zeolity-clinoptilolite-as a sorbent. *Environ. Prot. Eng.* **2013**, *39*, 139–152. [[CrossRef](#)]
57. Banković, P.; Milutinović-Nikolić, A.; Mojović, Z.; Jović-Jovičić, N.; Žunić, M.; Dondur, V.; Jovanović, D. Al,Fe-pillared clays in catalytic decolorization of aqueous tartrazine solutions. *Appl. Clay Sci.* **2012**, *58*, 73–78. [[CrossRef](#)]
58. Bieseki, L.; Treichel, H.; Araujo, A.S.; Pergher, S.B.C. Porous materials obtained by acid treatment processing followed by pillaring of montmorillonite clays. *Appl. Clay Sci.* **2013**, *85*, 46–52. [[CrossRef](#)]
59. Hernández-Huesca, R.; Díaz, L.; Aguilar-Armenta, G. Adsorption equilibria and kinetics of CO₂, CH₄ and N₂ in natural zeolites. *Sep. Purif. Technol.* **1999**, *15*, 163–173. [[CrossRef](#)]
60. Zhang, Y.; Qu, Y.; Wang, J. Effect of crystal size on the catalytic performance of HZSM-5 Zeolite in the methanol to aromatics reaction. *Pet. Sci. Technol.* **2018**, *36*, 898–903. [[CrossRef](#)]
61. Doula, M.; Ioannou, A.; Dimirkou, A. Copper adsorption and Si, Al, Ca, Mg, and Na release from clinoptilolite. *J. Colloid Interface Sci.* **2002**, *245*, 237–250. [[CrossRef](#)]
62. Doula, M.K. Synthesis of a clinoptilolite-Fe system with high Cu sorption capacity. *Chemosphere* **2007**, *67*, 731–740. [[CrossRef](#)] [[PubMed](#)]
63. Doula, M.K.; Ioannou, A. The effect of electrolyte anion on Cu adsorption-desorption by clinoptilolite. *Microporous Mesoporous Mater.* **2003**, *58*, 115–130. [[CrossRef](#)]
64. Yang, C.; Xu, Q. States of aluminum in zeolite β and influence of acidic or basic medium. *Zeolites* **1997**, *19*, 404–410. [[CrossRef](#)]
65. Kumar, M.S.; Schwidder, M.; Grünert, W.; Brückner, A. On the nature of different iron sites and their catalytic role in Fe-ZSM-5 DeNO_x catalysts: New insights by a combined EPR and UV/VIS spectroscopic approach. *J. Catal.* **2004**, *227*, 384–397. [[CrossRef](#)]
66. Gurgul, J.; Łątka, K.; Hnat, I.; Rynkowski, J.; Dzwigaj, S. Identification of iron species in FeSiBEA by DR UV-vis, XPS and Mössbauer spectroscopy: Influence of Fe content. *Microporous Mesoporous Mater.* **2013**, *168*, 1–6. [[CrossRef](#)]
67. Schwidder, M.; Heikens, S.; De Toni, A.; Geisler, S.; Berndt, M.; Brückner, A.; Grünert, W. The role of NO₂ in the selective catalytic reduction of nitrogen oxides over Fe-ZSM-5 catalysts: Active sites for the conversion of NO and of NO/NO₂ mixtures. *J. Catal.* **2008**, *259*, 96–103. [[CrossRef](#)]
68. Chen, J.; Gang, P.; Zheng, W.; Zhang, W.; Li, G.; Wu, X. Excellent performance of one-pot synthesized Fe-containing MCM-22 zeolites for the selective catalytic reduction of NO_x with NH₃. *Catal. Sci.* **2020**, *10*, 6583–6598. [[CrossRef](#)]